Improved integrating-sphere throughput with a lens and nonimaging concentrator

David B. Chenault, Keith A. Snail, and Leonard M. Hanssen

A reflectometer design utilizing an integrating sphere with a lens and nonimaging concentrator is described. Compared with previous designs where a collimator was used to restrict the detector field of view, the concentrator–lens combination significantly increases the throughput of the reflectometer. A procedure for designing lens–concentrators is given along with the results of parametric studies. The measured angular response of a lens–concentrator system is compared with ray-trace predictions and with the response of an ideal system. © 1995 Optical Society of America

1. Introduction

In many designs of integrating-sphere reflectometers, it is often implicitly assumed that the detector field of view (FOV) is hemispherical. In the IR a combination of weak radiation sources and low integrating-sphere efficiencies necessitates the use of cryogenically cooled photoconductive detectors. Cooled detectors (e.g., HgCdTe and InSb) do not have hemispherical FOV's because of Fresnel effects associated with all detectors and also the physical constraints of the dewar and cold shields. If a restricted FOV detector is used in an IR sphere, which is designed for a hemispherical FOV detector, significant measurement errors can result.[1,2] Early in this century, Taylor[3] and Sharp and Little[4] provided the solution to this type of problem. They proposed restricting the detector FOV in a controlled fashion by baffling either the detector FOV from the sample ($0/d$ geometry) or the input beam spot from the detector ($d/0$ geometry). An alternative to baffling is to restrict the detector's FOV with a collimator and lens. Restricting the FOV of the detector with a baffle or callimetor can significantly reduce the overall throughput of an integrating sphere,[5] and hence these sphere designs have found limited applications.[6]

D. B. Chenault and K. A. Snail are with the Optical Sciences ~~Division, Cod~~e 5622, U.S. Naval Research Laboratory, Washington, D.C. 20375-5320. L. M. Hanssen is with the Radiometric Physics Division, National Institute of Standards and Technology, Gaithersburg, Maryland 20899.

Received 9 December 1994; revised manuscript received 7 July 1995.

0003-6935/95/347959-06$06.00/0.

© 1995 Optical Society of America.

Recently, Lang and Masterson,[7] Tardy,[8] and Snail and Hanssen[2] have shown that nonimaging concentrators could be used to restrict the detector FOV in integrating spheres without sacrificing throughput. Nonimaging concentrators were first developed for the detection of Cherenkov radiation.[9] They have been applied to many light-collection applications, such as the solar-energy collection[10] and the far-IR light collection,[11] and are well suited for use with integrating spheres. The advantages of using a nonimaging concentrator with an IR integrating sphere are the following: (1) The detector FOV can be varied with negligible loss in throughput. (2) The detector FOV can be sharply defined. (3) The light rejected by the concentrator is returned to the sphere. It is important to limit the detector FOV to view only a small part of the integrating sphere wall. Such an arrangement helps to reduce the size of the baffles in the sphere, which preserves the symmetry of the sphere and simplifies modeling the response of the sphere for correlation with calibration samples.

Several types of nonimaging concentrator can be applied to integrating-sphere designs.[2] Compound elliptic concentrators (CEC's) and compound parabolic concentrators (CPC's) have been used to restrict detector FOV's.[8] However, because the CPC and CEC lengths scale as the square of the concentration, narrow FOV's such as those required in the sphere designs of Taylor[3] and Sharp and Little[4] result in impractically long concentrators[8] that cannot easily be attached to a dewar's cold finger for low-temperature operation. An alternative approach utilizes a nonimaging compound hyperbolic concentrator (CHC) and a lens in combination.[10] The length of the CHC–lens system scales only as the concentration and hence is substantially smaller than the equiva-

lent CEC or CPC. This permits the concentrator to be mounted directly to the dewar's cold finger with the lens serving as the dewar window.

In the nonimaging concentrator detection scheme, light entering the concentrator from outside the detector FOV is rejected and returned to the sphere, thus enhancing the sphere throughput. For identically sized detectors and FOV's an integrating-sphere employing a collimator will have a throughput that is lower than a sphere with a nonimaging concentrator by a factor[8] of

$$4y_x^2/\{[(y_e + y_x)^2 + Q^2]^{1/2} - [(y_e - y_x)^2 + Q^2]^{1/2}\}^2,$$

where y_e is the collimator radius, y_x is the detector radius, and Q is the collimator length. For a $\pm 10°$ half-angle detector FOV, which is typical of the Taylor and Sharp–Little designs, the throughput enhancement of the nonimaging concentrator is ~30. Note, however, that this relation does not include an additional enhancement of the throughput because of the light outside the FOV that is returned to the sphere. Nor does this relation include a small reduction in the throughput because of the finite absorption of the CHC, the finite transmittance of the lens, and the Fresnel response of the detector.

In Section 2 we describe the design of the CHC and lens for an integrating sphere. Initially, we assume that the lens is an ideal lens, the CHC is 100% reflecting, and the detector absorbs all the incident radiation. The second stage of the design incorporates the aberration and the Fresnel effects of a real lens and reasonable values for the reflectance and absorptance of the CHC and detector. The final design and predicted response of the system are determined by a comprehensive ray trace of the system. In Section 3 we describe the measured performance of the CHC and lens and compare it with the predicted performance. In Section 4 we summarize the performance advantages and describe future directions for this research.

2. Integrating Sphere–Nonimaging Concentrator Geometry

A. Ideal CHC and Lens

An integrating sphere with a lens and CHC is shown in Fig. 1. The entrance port of the sphere is at the top with the sample and reference at the bottom. Only the sample is shown in this figure; the reference port is beyond the plane of the page. The area of the sphere wall that lies in the detector FOV is on the left. The lens, CHC, and detector are shown on the right. The angle of incidence θ of light incident on the lens from a point on the sphere wall is measured with respect to the optic axis of the CHC–lens. The shape of the CHC depends on the focal length of the lens, the entrance- and exit-aperture sizes, the sphere diameter, and the detector FOV.

The edge-ray method of the nonimaging optics design[9] is used to determine the shape of the CHC

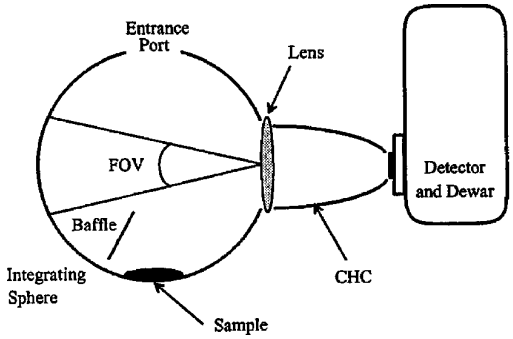

Fig. 1. Integrating-sphere reflectometer with CHC, lens, detector, and baffle.

based on the other system parameters. Figure 2 shows an ideal lens and the CHC with meridonal rays incident from the edge of the detector FOV on the sphere wall. The ideal lens is assumed to have no aberrations with 100% transmission and to be infinitely thin. The integrating sphere has a radius R. The entrance aperture to the CHC is $E'E$, the exit aperture is HF_2, and the optic axis of the CHC–lens systems is $O''O$, where O is the origin of the y–z coordinate system. The distance from the point at the edge of the detector FOV on the sphere wall and the plane of the lens is S_1. The distance from the plane of the lens to the image point F_1 is S_2. The CHC mirror is now placed in front of point F_1 so that the light comes to a focus at point F_2. Points F_1 and F_2 are the foci of the hyperbola shown by curve $H'H$. The section of the hyperbola limited by the entrance aperture of the concentrator (or lens) and the exit aperture (or detector) is rotated about the optical axis of the lens to form a hyperboloid of revolution. The length Q of the CHC, expressed in terms of S_1 and S_2, the entrance- and exit-aperture radii $y_e\,(E'E/2)$ and $y_x\,(HF_2/2)$, and the radius of the FOV on the sphere wall $y_c\,(C'C/2)$ are given by

$$Q = \frac{y_e + y_x}{\dfrac{y_c}{S_1} + \dfrac{y_e}{S_2}}. \tag{1}$$

The equation of the hyperbola in the primed coordi-

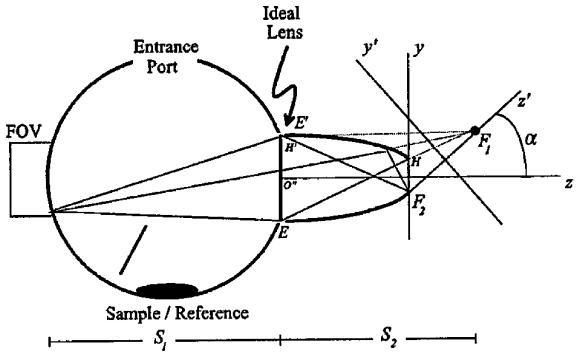

Fig. 2. Geometry of the integrating sphere, the CHC, and the ideal lens for the edge-ray design process.

nate frame is given by

$$\frac{z'^2}{a^2} - \frac{y'^2}{b^2} = 1. \tag{2}$$

Coefficients a and b, written in terms of S_1 and S_2, the entrance- and exit-aperture radii y_e and y_x, the length of the CHC Q, and the radius of the FOV on the sphere wall y_c are

$$a = \frac{1}{2}\left[(S_2 - Q)^2 + \left(y_c \frac{S_2}{S_1} - y_x\right)^2\right]^{1/2} - y_x,$$

$$c = \frac{1}{2}\left[(S_2 - Q)^2 + \left(y_c \frac{S_2}{S_1} + y_x\right)^2\right]^{1/2}, \quad b = (c^2 - a^2)^{1/2}. \tag{3}$$

The coordinates of the origin of the primed frame in the unprimed frame are

$$z_0 = c \cos \alpha, \qquad y_0 = c \sin \alpha - y_x, \tag{4}$$

where

$$\alpha = a \tan\left(\frac{\frac{y_c}{S_1} + \frac{y_x}{S_2}}{1 - \frac{Q}{S_2}}\right) \tag{5}$$

is the angle that the primed coordinate system makes with the unprimed system. The transformation from the unprimed to primed coordinate system is given by translation and rotation,

$$z' = (z - z_0)\cos \alpha + (y - y_0)\sin \alpha,$$
$$y' = (y - y_0)\cos \alpha - (z - z_0)\sin \alpha. \tag{6}$$

We then obtain a numerical solution by solving the equation of the hyperbola [Eq. (2)] for the FOV radius y_c given values for the other parameters of the system. In our parametric studies we fixed the radius of the sphere, the entrance and exit apertures of the CHC, and the focal length of the lens. The sphere radius R and focal length f are sufficient to determine object and image distances S_1 and S_2. The exit aperture can be fixed with consideration for the size of the detector that will be used in the system. The CHC entrance aperture is chosen to keep the total port area in the sphere below 5% of the sphere wall area. These values and Eqs. (1), (3), (4), and (6) in Eq. (2) give a relation in y_c that is easily solved numerically given the fixed point on the hyperbola $(z, y) = (-Q, y_e)$. The FOV half-angle is then

$$\theta = \tan^{-1}\left(\frac{y_c}{S_1}\right). \tag{7}$$

Parametric studies indicate that the length of the CHC increases for both the increasing entrance-aperture diameter and increasing focal length, as shown in Fig. 3. The concentrator FOV was chosen to be as large as possible, so that a baffle can still be placed between the sample and FOV without protruding into the beam path or the detector FOV. The baffle is assumed to be specular and to lie in a plane containing a great circle of the sphere. Table 1 shows the values of the parameters chosen as suitable for a 12.7- and a 15.2-cm-diameter IR integrating-sphere reflectometer.

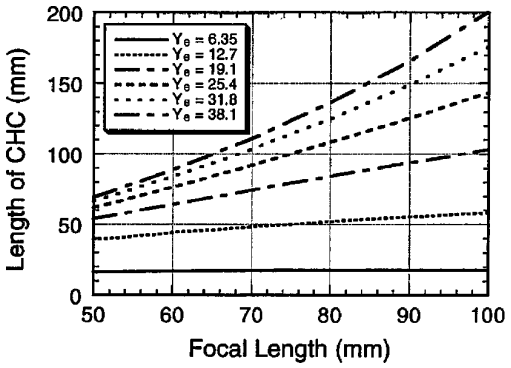

Fig. 3. Length of the CHC as a function of the lens focal length for various lens radii, assuming a 6-mm-diameter CHC exit aperture and a 12.7-cm-diameter integrating sphere.

To confirm the design and to determine the sharpness of the cutoff at the edge of the FOV, a series of ray traces was performed on the system. For each ray trace a grid of rays that just fills the clear aperture of the lens is traced from a point on the sphere wall at a given angle of incidence until the ray is either absorbed by the detector or turned back by the CHC. The angle of incidence is measured relative to the normal of the entrance aperture of the CHC. Note that in the ray trace the grid of rays includes skew rays,[9] which will not necessarily behave as the edge rays in the design process. These rays tend to broaden the angular response of the lens and the CHC. Figure 4 shows an example ray trace of the 12.7-cm sphere with three rays at 0° [Fig. 4(a)], 5° [Fig. 4(b)], 15° [Fig. 4(c)], and 45° [Fig. 4(d)]. The cutoff angle is 10.2° for this sphere. Note that all the rays are turned back by the concentrator at the two larger angles of incidence. Figure 5 shows the normalized flux incident on the detector as a function of the incident angle, as determined from ray tracing. The throughput exhibits a slight rounding around the cutoff angle caused by skew-ray effects.

Table 1. Design Parameters for IR Integrating Spheres with a CHC–Lens

Design Parameter	Design 1	Design 2
Diameter of sphere (mm)	127	152.4
CHC entrance-aperture diameter, $2y_e$ (mm)	32	23.4
CHC exit-aperture diameter, $2y_x$ (mm)	5.6	5.6
Focal length of lens (mm)	57	75.7
FOV half-angle (deg)	10.2	13.8
CHC length (mm)	53.2	44

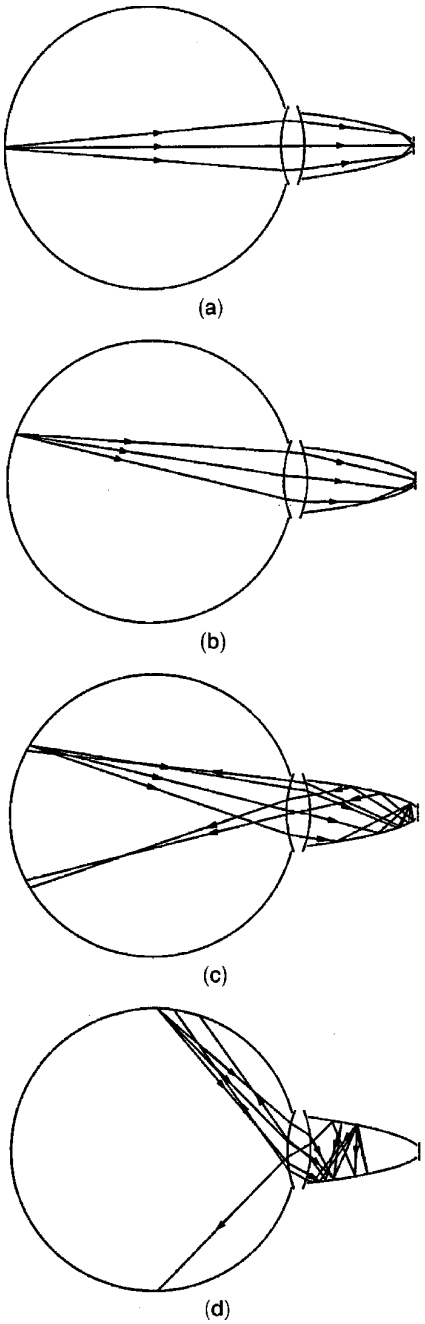

Fig. 4. Ray traces of three meridional rays through a CHC–lens with a 10.2° cutoff angle for incident angles of (a) 0°, (b) 5°, (c) 15°, and (d) 45°.

B. Real CHC and Lens

The design and analysis in Subsection 2.A shows that the CHC and lens combination performs as needed for the integrating-sphere application, assuming that the lens and CHC are ideal. We now expand the analysis by assuming appropriate materials for the lens, the CHC mirror, and the detector. The aberrations and the Fresnel effects of the lens, the nonideal reflectivity of the mirror, and the Fresnel effects of the detector are incorporated into the ray-tracing analysis of the system, and a more realistic measure of system performance is determined.

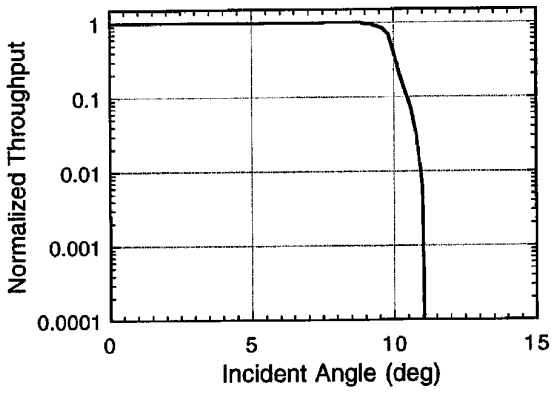

Fig. 5. Predicted angular throughput of a CHC–ideal lens system designed for the 12.7-cm-diameter sphere.

The Fresnel effects of the lens and the detector are the major contributors to misdirected rays in the CHC and lens system. There are two situations in which the multiple reflections of the lens are potentially detrimental to the performance of the integrating sphere: (1) the incident light lies within the FOV and light is reflected back out of the CHC and falls outside the detector FOV in the integrating sphere; (2) the incident light lies outside the FOV and the multiple reflections cause light that should be rejected to be reflected back into the CHC and to fall on the detector. The first situation results in only a slight reduction in throughput for these rays because the light remains in the system. In the second situation the light that is detected could result in significant errors. For example, an apparent increase in the reflectance of the sample could result if the bidirectional reflectance distribution function of the sample is such that a large fraction of the light incident on the sample is reflected directly onto the lens (i.e., at a 45° incident angle).

The Fresnel effects of the detector become important when the angles of incidence on the detector become large. For rays near the edge of the FOV of the lens and CHC system, the angle of incidence of these rays on the detector increase, resulting in an increase in reflected intensity. This tends to reduce the throughput of the lens and CHC near the edge of the FOV. Snail and Carr[5] analyzed this effect, however, and concluded that for HgCdTe the loss in throughput is small.

Additional effects that degrade the performance of the lens and CHC system are the gaps between the detector surface and CHC and between the CHC and the lens. Although these effects should be minimized, some trade-offs between the optical and mechanical design must be accepted. In our system design the lens acts as the window on the dewar, and the CHC is cooled to liquid nitrogen temperatures. Heat transfer between the two should be minimized while the gap is also minimized. Excessive heat transfer could result in unwanted stress on the lens, condensation on the lens, and excessive detected noise caused by warming of the CHC.

Another effect that reduces the performance of the lens and CHC relative to the ideal design is the reflection losses of the CHC. There can be a large number of reflections for rays near the edge of the FOV and for skew rays. The throughput of these rays is reduced if the reflectivity of the CHC becomes significantly less than 1. Aluminum and gold are therefore good choices for the CHC in the IR because of their relatively high reflectivity.

A CHC and lens were designed as described above. The lens material chosen was potassium chloride, which has one of the lowest refractive indices of IR lens materials and is the most suitable for reducing the Fresnel effects of the lens. A stock lens was chosen to reduce cost. Compatibility of the focal length with the other system parameters was confirmed by parametric and ray-tracing studies.

In Figs. 6(a) and 6(b) we show the results of ray traces of the CHC–lens system developed for the 12.7- and 15.2-cm-diameter spheres, using standard values for the detector, mirror, and lens[12] optical constants. The ray-traced data are shown by the dotted curves. The ray grid consisted of ~8000 rays, and ray tracing was done at 2-deg intervals for incident angles of >20° and 1-deg intervals for incident angles of <20°. The structure in the ray-traced data outside the acceptance angle is due to multiple-reflection effects in the lens. The average throughput outside the FOV is more than 2 orders of magnitude lower than the throughput inside the FOV.

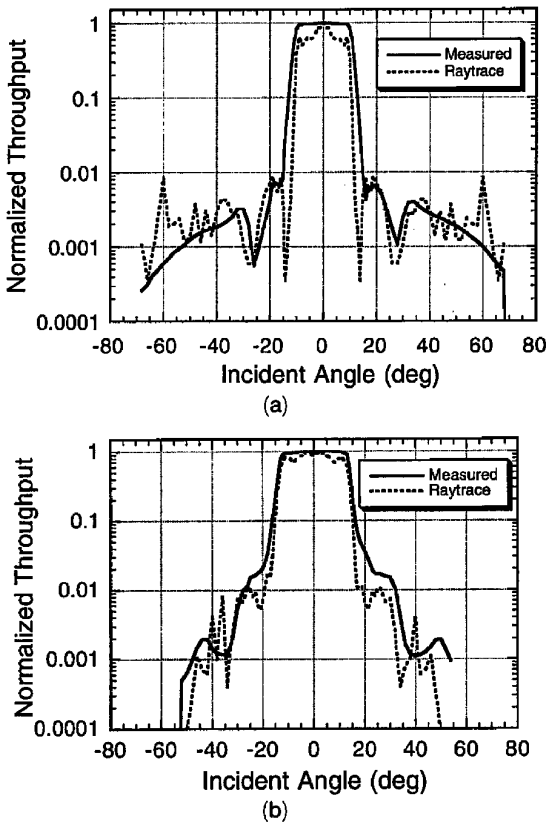

Fig. 6. (a) Comparison of the predicted (ray trace) and the measured throughput versus the incident angle of the CHC–lens for the 12.7-cm-diameter integrating sphere. (b) Comparison of the predicted (ray trace) and the measured throughput versus the incident angle of the CHC–lens for the 15.2-cm-diameter integrating sphere.

3. Performance of an IR CHC and Lens

The nonimaging CHC's described in Subsection 2.B were fabricated and mounted in front of 6-mm-diameter HgCdTe detector elements. For the 12.7-cm sphere the CHC was diamond-turned with a final groove separation of <2 μm to reduce scatter. The CHC for the 15.2-cm sphere was fabricated out of electroplated nickel with a polished stainless steel mandril and was gold coated. The lenses were mounted in aluminum sleeves that were coupled to the outer wall of the dewar with an O-ring seal.

The lens–CHC assemblies were tested at 10.6 μm to confirm the angular performance. The output beam of a CO_2 laser was attenuated and chopped. The laser beam was expanded to slightly underfill the entrance aperture of the lens. The beam divergence was ~5°. Output voltages from the HgCdTe elements were read from a lockin amplifier referenced to a pyroelectric detector. The uncertainty of these measurements was ±0.3%.

The CHC and lens were mounted so that the incident light on the lens could be varied from 0° to 70° to simulate light reflected from various points on the sphere wall onto the lens. Measurements were made in 1° increments (±0.1°) from 0° to 20° and in 2° increments beyond 20°. The measured angular response is compared with ray-trace results for the 12.7-cm sphere in Fig. 6(a) and the 15.2-cm sphere in Fig. 6(b). The measured data are smoother than the ray trace because of the beam divergence and the relatively small number of rays traced in the ray grid. The data display the same dip at 26° and an indication of the dip at 15°. There is an apparent broadening of the FOV by ~2°, but the throughput response outside the FOV is more than 2 orders of magnitude below that inside the FOV. When a detector with a nonimaging concentrator is used with an integrating sphere, the variations in throughput inside the FOV will be averaged out by the sphere's tendency to illuminate all parts of the FOV uniformly after each wall reflection.

4. Summary

A design for an integrating sphere utilizing a lens and nonimaging CHC has been presented. The CHC and lens restrict the FOV of the detector with minimal loss in the throughput of the integrating sphere. The CHC and lens should exhibit excellent uniformity of throughput inside the detector FOV while efficiently rejecting the light entering from outside the FOV. The angular throughput performance has been confirmed by ray tracing and by measurements of the assembled system. The ray-trace results show more structure than the measurements, but this is most likely a result of the limitations to the number of rays in the ray trace and the divergence of the

experimental beam. The throughput outside the FOV is 2 orders of magnitude less than the throughput inside the FOV, and the angular cutoff occurs over less than 2°.

An IR integrating sphere with a CHC and a lens has been fabricated and is currently being evaluated. The throughput performance of the CHC and lens systems is ideal for application in an integrating sphere and should improve the sphere's performance both in terms of its throughput and in reducing its sensitivity to the sample bidirectional reflectance distribution function. Future research will focus on the performance of the CHC and lens with the IR integrating sphere, and nonhyperbolic concentrator designs for correcting for lens aberrations will be investigated.

The authors thank the Office of Naval Technology and Naval Warfare Assessment Department in Corona, Calif. for partial support of this effort.

References

1. L. M. Hanssen, "Effects of restricting the detector field of view when using integrating sphere," Appl. Opt. **28,** 2097–2103 (1989).
2. K. A. Snail and L. M. Hanssen, "Integrating sphere designs with isotropic throughput," Appl. Opt. **28,** 1793–1799 (1989).
3. A. H. Taylor, "A simple portable instrument for measuring reflection and transmission factors in absolute units," Trans. IES **15,** 811–826 (1920).
4. C. H. Sharp and W. F. Little, "Measurement of reflection factors," Trans. IES **15,** 802–810 (1920).
5. K. A. Snail and K. F. Carr, "Optical design of an integrating sphere–Fourier transform spectrometer (FTS) reflectometer," in *Infrared, Adaptive, and Synthetic Aperture Optical Systems*, J. S. Fender, R. B. Johnson, and W. L. Wolfe, eds., Proc. Soc. Photo-Opt. Instrum. Eng. **643,** 75–83 (1986).
6. W. Richter, "Fourier transform reflectance spectrometry between 8000 cm^{-1} (1.25 μm) and 800 cm^{-1} (12.5 μm) using an integrating sphere," Appl. Spectrosc. **37,** 32–38 (1983).
7. M. G. Lang and K. D. Masterson, "Compound ellipsoid concentrator baffle integrating sphere," J. Opt. Soc. Am. **70,** 1564 (1980).
8. H. L. Tardy, "Flux concentrators in integrating spheres experiments: potential for increased detector signal," Appl. Opt. **24,** 3914–3916 (1985).
9. W. W. Welford and R. Winston, *High Collection Nonimaging Optics* (Academic, New York, 1978).
10. M. Collares-Pereira, A. Rabl, and R. Winston, "Lens–mirror combinations with maximal concentration," Appl. Opt. **16,** 2677–2683 (1977).
11. D. A. Harper, R. H. Hildebrand, R. Stiening, and R. Winston, "Heat trap: an optimized far infrared field optics system," Appl. Opt. **15,** 53–59 (1976).
12. E. D. Palik, "Potassium chloride," in *Handbook of Optical Constants of Solids*, E. D. Palik, ed. (Academic, New York, 1985), pp. 703–706.